Synaptic Connectivity of Afferent Inputs onto Projection Neurons in the Songbird HVC

Massimo Trusel, Danyal Alam and Todd F. Roberts*
Department of Neuroscience, UT Southwestern Medical Center, Dallas TX, USA
Correspondence should be addressed to TFR, Todd.Roberts@utsouthwestern.edu

Abstract

Birdsong is a complex and volitionally produced skilled behavior that, like speech and language, is dependent on forebrain circuits for its fluent production. The well delineated neural circuits associated with song provide a powerful system in which to study how synaptically linked networks of neurons control a natural and complex behavior. The premotor cortical analog HVC is necessary for song production and for song learning. Although the main input and output pathways of HVC have in most cases been known for decades, we still lack a detailed synaptic wiring diagram of this core circuit. Here we report our progress in building this wiring diagram. HVC has at least three non-overlapping classes of projection neurons and receives input from at least five song associated regions – totaling 15 potential synaptic pathways. Combining optogenetic stimulation of axon terminals from HVC's different afferent pathways with targeted whole-cell patch-clamp recordings of HVC projection neurons, we now provide an initial synaptic connectivity map of 12 of these potential pathways. We report on 435 whole-cell patch-clamp recordings from the 3 classes of HVC projection neurons, examining 4 different input pathways, from NIf, Uva, mMAN, Av, and mapping the polysynaptic and monosynaptic connections in each pathway. We find that the synaptic connectivity of HVC's input-output pathways is complex. Each class of projection neuron receives monosynaptic input from three of the four afferents and all in different combinations. At this stage, only one input pathway, NIf, appears to monosynaptically project onto all three classes of HVC projection neurons. We provide this initial synaptic mapping as an update for the field and will build on this wiring diagram, by updating this bioRxiv manuscript, as more data is collected, and additional pathways are characterized.

Introduction

The courtship song of male zebra finches is one of the better studied naturally learned behaviors[1-12]. This song is controlled by a relatively discrete set of interconnected forebrain regions[13-19]. The premotor cortical analog HVC (proper name) is a central hub in this song network. HVC is necessary for song production and serves as the primary interface between auditory/proprioceptive feedback circuits, and the premotor circuits involved in learning and controlling singing behavior. HVC receives intra-telencephalic input from 4 sensory and sensorimotor regions (NIf, Av, mMAN and RA) and one thalamic brain region, Uva (**Fig. 1A-B**, see Fig.1 legend for anatomical descriptions). Several lines of evidence now support the idea that song control involves some of these pathways projecting into HVC[19-24]. In addition, HVC has anatomically separable output pathways onto the descending song motor pathway (HVC's projection onto RA through HVC_{RA} neurons), the basal ganglia (HVC's projection onto Area X through HVC_X neurons), and the auditory forebrain (HVC's projection onto Avalanche through HVC_{Av} neurons)[19].

Mapping the synaptic connectivity between HVC's input and output pathways has been hindered by the lack of appropriate tools for robustly manipulating these circuits in the songbird brain, an issue we have overcome by employing better performing optogenetic channels packaged in an adeno associated virus (AAV) that we optimized for expression throughout various portions of the song circuitry. Specifically, we made use of the axonal expression of the opsin eGtACR1[25,26]. GtACRs are blue light-driven Cl^- channels that, while hyperpolarizing at the soma and dendrites, are reportedly depolarizing at axon terminals due to the shifted internal Cl^- concentration in axonal compartments[27-29]. We applied this strategy to achieve independent control of synaptic release from NIf, Uva, mMAN, and Av. We paired this with whole cell patch-clamp recordings from visually targeted HVC projection neurons (HVC-PNs; HVC_X, HVC_{RA}, HVC_{Av}), identified using retrograde tracer injections into each efferent region (**Fig. 1C**). This allowed us to study the properties of synaptic transmission at 12 specific afferent-HVC-PN combinations.

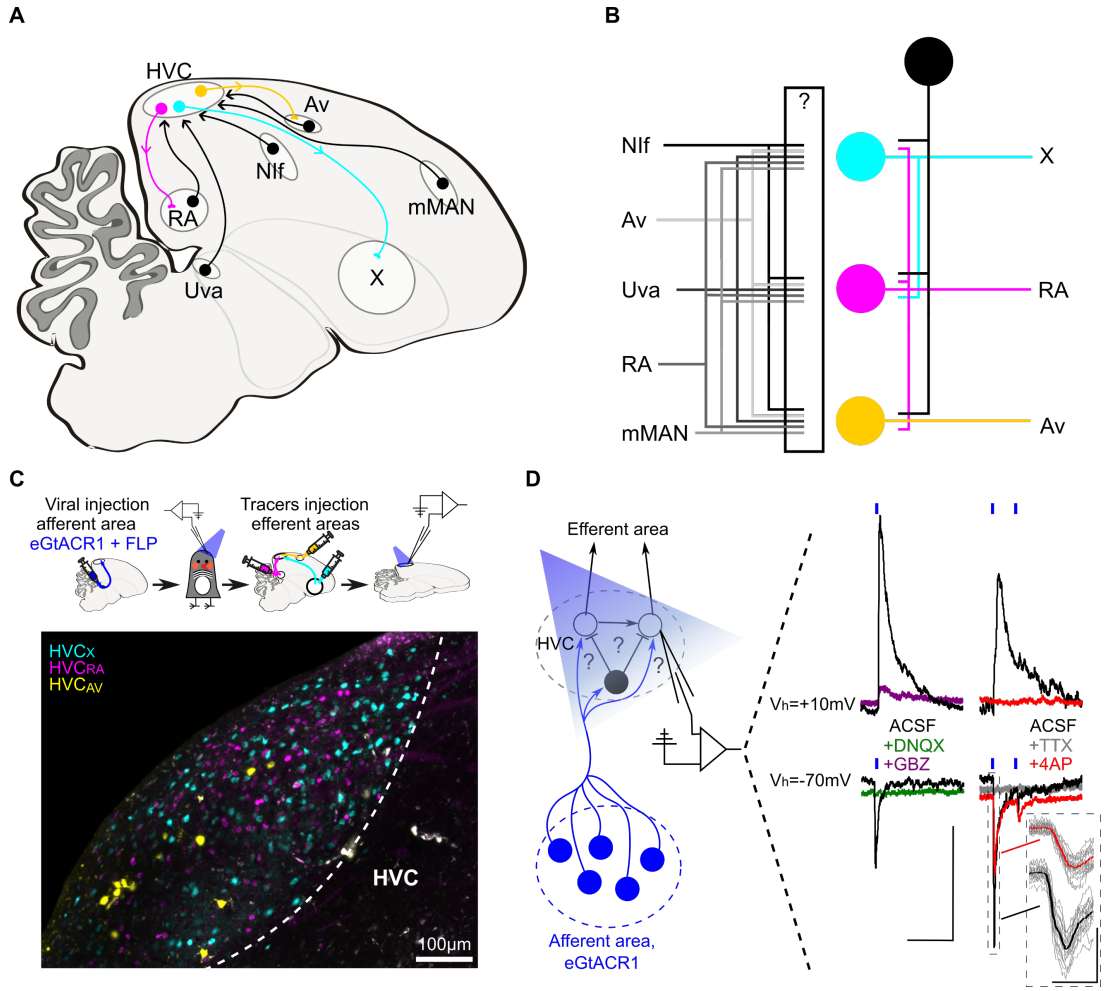

Fig. 1: Strategy for opsin assisted HVC circuit mapping. A) *Parasagittal schematic of the zebra finch brain illustrating HVC afferents (black) from nucleus interface of the nidopallium (NIf), nucleus avalanche (Av), medial magnocellular nucleus of the anterior nidopallium (mMAN), nucleus Uvaeformis (Uva) and robust nucleus of the arcopallium (RA), as well as the HVC-PN classes* HVC_X *(projecting to area X, cyan),* HVC_{RA} *(projecting to RA, magenta) and* HVC_{Av} *(projecting to Av, yellow).* ***B)*** *schematic portraying the unknown detailed synaptic map of afferents to HVC (focus on projections to HVC-PNs,* HVC_X *cyan,* HVC_{RA} *magenta,* HVC_{Av} *yellow. HVC interneurons schematized in black).* ***C)*** *(top) schematic of the workflow for each bird, including opsin expression in afferent areas, in-vivo anesthetized extracellular recording of optically evoked currents, injection of retrograde tracers (1-3, depending on the experimental needs) in HVC efferents and ultimately whole cell patch-clamp recording of optically evoked currents in acute brain slices. (bottom) sample image of HVC-PN classes in a brain slice used for patch-clamp recordings (*HVC_X *cyan,* HVC_{RA} *magenta,* HVC_{Av} *yellow, scalebar 100µm).* ***D)*** *schematic of whole-cell recording of optically evoked currents in HVC-PNs (unfilled circles) receiving monosynaptic inputs from one of the afferent areas expressing eGtACR1, as well as polysynaptic inputs from local HVC-PNs and interneurons (black circle). Recordings are performed at +10mV and -70mV. Sample traces report the effect of bath application of DNQX and gabazine (GBZ), which suppress oEPSC and oIPSC, respectively. Monosynaptic currents are pharmacologically isolated by bath application of TTX+4AP: sample traces show a typical case of a cell displaying oEPSC with a monosynaptic component, and polysynaptic oIPSC. 4AP application results in a partial restoration of oEPSC, but not of oIPSC (blue lines represent optical stimuli, 1ms; scalebar: 100ms, 100pA). Inset shows magnification of the polysynaptic and monosynaptic oEPSC (20 traces in gray, average traces in black and red, respectively), with a focus on the rise phase of the oEPSC. In ACSF (polysynaptic response) the slope displays a double peak. Upon application of TTX+4AP the oEPSC rise phase is monotonic, consistent with isolation of monosynaptic responses (scalebar: 5ms, 100pA).*

Results

To conduct our opsin-assisted circuit mapping, we expressed eGtACR1 in either NIf, Uva, mMAN, or Av using AAV (Fig. **1C**; a cocktail of AAV2.9-Cbh-FLP and AAV2.9-Cbh-fDIO-eGtACR1 injected in HVC afferent areas). 4-6 weeks later we performed in-vivo multiunit extracellular recordings from HVC in anesthetized birds to test for presence of robust optically evoked responses from excitation of individual input pathways. Birds exhibiting strong optogenetic responses received retrograde tracer injections in HVC projection areas (RA, Area X, and Av) to label HVC-PN classes in different fluorescent channels. Lastly, we obtained acute brain slices and performed patch-clamp recordings from HVC-PNs to examine optically evoked post-synaptic currents (oPSCs). We confirmed that oPSCs measured while holding the membrane voltage at -70mV were excitatory (oEPSCs) and mediated by AMPA receptors (current suppressed by bath application of DNQX; Fig. **1D**). Holding the membrane potential to +10mV allowed us to measure inhibitory currents (oIPSCs) mediated by GABAa receptors (current suppressed by bath application of gabazine; Fig. **1D**).

To reliably measure and compare synaptic properties across the various input-output pathways we set the optical stimulation intensity to achieve oEPSCs with an amplitude in the range of ~100-600pA. In a few cases currents either greatly exceeded or could not meet this threshold. For particularly strong currents we reduced the light intensity to achieve oEPSCs at ~50% of their maximal response. In cases with currents below 100pA we had to settle for amplitudes as low as ~30pA.

At this time, we are reporting on the likelihood of observing oEPSCs and oIPSCs, the amplitude of oEPSCs and oIPSCs, the paired-pulse ratio of the oEPSCs (PPR, 2 pulses spaced by 50ms), and the excitatory-inhibitory ratio (oEPSC/oIPSC) at each synaptic contact examined. We also tested whether observed synaptic currents had a monosynaptic component by sequentially applying tetrodotoxin (TTX) followed by 4-aminopiridyne (4AP)[30,31] (Fig. **1D**). We consistently observed that, while oEPSCs registered in ACSF displayed multiple peaks consistent with a polysynaptic source, currents were eliminated in the presence of TTX. Currents that returned following wash on of 4AP had a monotonic rising slope and a single peak, consistent with a monosynaptic origin of each current (Fig. **1D**).

Although opsin assisted circuit mapping provides a powerful approach for testing synaptic connectivity, there are a few general limitations of the approach that need to be considered at the outset. First, the amplitude and likelihood of recording oPSCs directly depends on the expression rate and tropism of our viruses and this may differ in subtle ways across the 4 pathways we report on here. Second, measurement of optically evoked PPR at 50ms should be interpreted cautiously because of the off kinetics of eGtACR1[32,33]. Lastly, there are intrinsic limitations to mapping synaptic connectivity in brain slices due to the potential of severing dendrites and other neuronal processes.

NIf provides excitatory monosynaptic input to all HVC-PNs.

We first probed the synaptic transmission between the auditory nucleus NIf and the 3 classes of HVC-PNs. We injected a cocktail of AAV-CBh-DIO-eGTACR1 and AAV-CBh-FLP in NIf (**Fig. 2A**). 4-6 weeks later we measured the change in HVC extracellular activity in-vivo upon optical stimulation of NIf axonal projections (473nm, 20mW, 1s). We found that blue light stimulation resulted in a significant increase in HVC spiking activity (last 100ms baseline vs. last 100ms stim, Wilcoxon matched-pairs signed rank test, $P < 0.0001$, **Fig. 2B**), indicative of opsin expression in the NIf terminals reaching HVC.

In acute brain slices, we reliably observed glutamatergic oEPSCs in all three classes of projection neurons (74.7% probability (53/71 cells): **HVC_X,** 85.7% probability (24/28 cells), average amplitude 277.5±43.2 pA; **HVC_{RA},** 70.8% probability (17/24 cells), average amplitude 146.3±85.9 pA; **HVC_{Av}**, 63.2% probability (12/19 cells), average amplitude 267.0±77.-0 pA. X^2 (2, n = 71) = 3.322, $P = 0.19$. Kruskal-Wallis test for oEPSC amplitude, H(2) = 2.815, $P = 0.2448$; **Fig. 2C**, **2D**).

In a subset of cells, we also tested whether oIPSCs could be observed. We found robust GABAergic currents evoked by optical stimulation in all three classes of projection neurons (60% probability (24/40 cells): **HVC_X**, 54.6% probability (6/11 cells), average amplitude 769.9±181.4 pA; **HVC_{RA}**, 66.7% probability (10/15 cells), average amplitude 426.1±126.7 pA; **HVC_{Av}**, 57.2% probability (8/14 cells), average amplitude 948.6±272.7 pA. X^2 (2, n = 40) = 0.4618, $P = 0.7938$; Kruskal-Wallis test, H(2) = 3.554, $P = 0.1692$; **Fig. 2E**). oIPSCs were predominantly present in cells where oEPSCs were also observed

(**HVC_X**, 54.5% oEPSC+oIPSC, 9.1% oEPSC without oIPSC, 36.4% neither oEPSC nor oIPSC; **HVC_{RA}**, 46.6% oEPSC+oIPSC, 6.7% oEPSC without oIPSC, 20% oIPSC without oEPSC, 26.7% neither oEPSC nor oIPSC; **HVC_{Av}**, 57.1% oEPSC+oIPSC, 42.9% neither oEPSC nor oIPSC; **Fig. 2C**).

The PPR was similar and < 1 in all 3 pathways, suggesting similarly high presynaptic vesicle release probability at NIf's inputs onto HVC projection neurons (**HVC_X**, 0.43±0.040; **HVC_{RA}**, 0.47±0.049; **HVC_{Av}**, 0.51±0.061; one-way Anova F(2,35) = 0.5775, *P* = 0.5666; **Fig. 2F**).

When calculating the excitation/inhibition ratio, we observed that optogenetic stimulation of NIf axonal terminals evoked relatively higher amplitude oIPSCs than oEPSCs in all cellular subtypes (**HVC_X**, 0.47±0.096; **HVC_{RA}**, 0.28±0.059; **HVC_{Av}**, 0.45±0.062; one-way Anova F(2,18) = 2.087, *P* = 0.1530; **Fig. 2G**).

Lastly, we examined if the observed neurotransmission from NIf to each HVC-PNs is monosynaptic or only polysynaptic. We observed that 4AP reliably restored oEPSCs in all three HVC projection subtypes (3/3 cells tested per each class; residual current after TTX+4AP application: **HVC_X,** 12.4±0.5%; **HVC_{RA},** 8.9±15.7%; **HVC_{Av},** 15±14%, **Fig. 2H**). oIPSCs were not observed after 4AP application: **HVC_X**, 0/3 cells tested; **HVC_{RA}**, 0/2 cells tested; **HVC_{Av}**, 0/1 cell tested). This finding is consistent with previous studies indicating that NIf projections result in disynaptic inhibition onto HVC projection neurons[34]. These results indicate that NIf provides excitatory monosynaptic projections onto all 3 known classes of HVC-PNs.

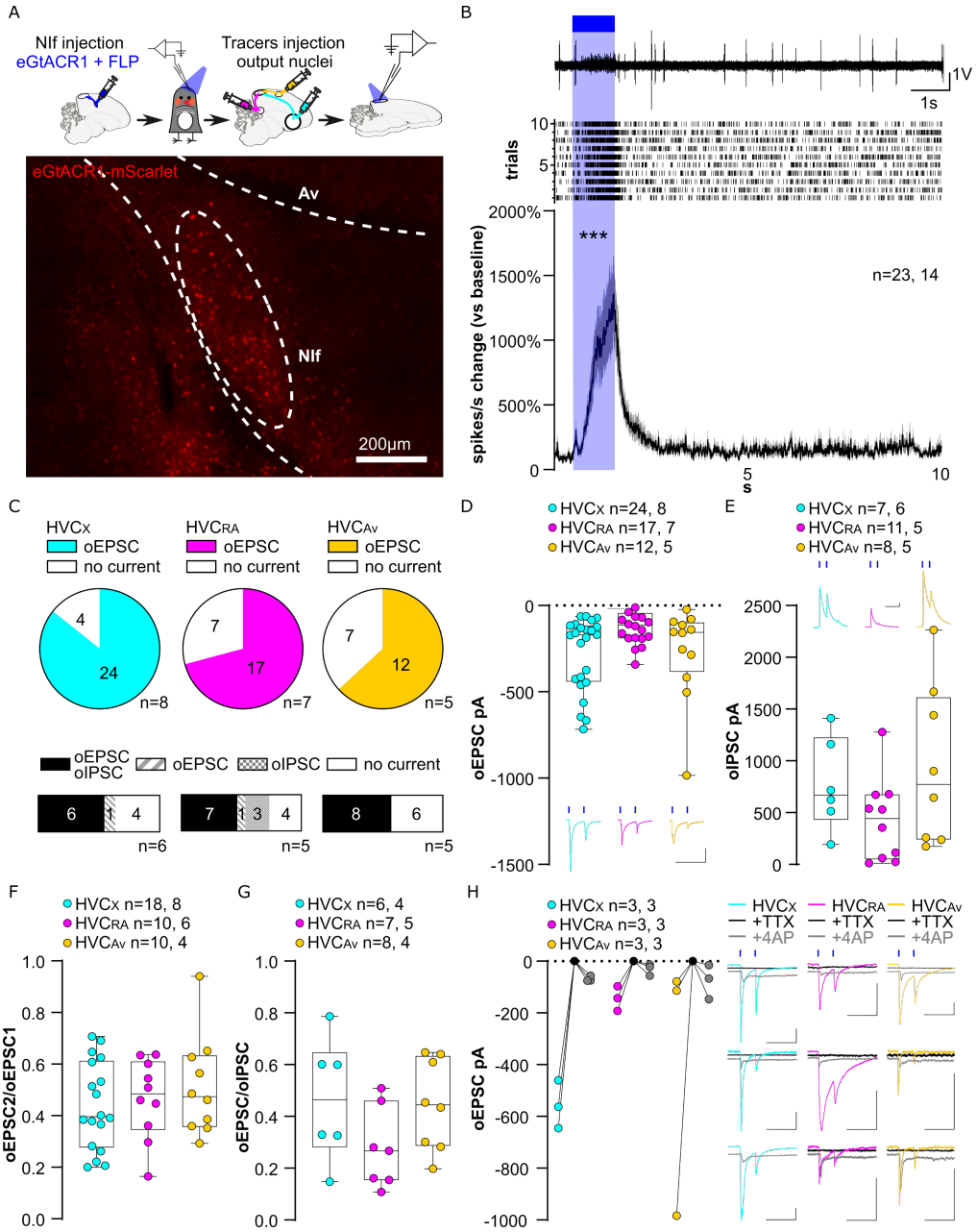

Fig. 2: Stimulation of NIf inputs to HVC reliably elicits polysynaptic oIPSCs and oEPSCs, and monosynaptic oEPSCs, in all three HVC-PN classes. A*) (top) Schematic of the experimental timeline, illustrating injection of AAV-CBh-DIO-eGtACR1+ AAV-CBh-FLP in NIf, followed by in-vivo extracellular recording of optically evoked HVC spiking activity in anesthetized birds, retrograde tracer injections in HVC efferent areas and whole-cell patch-clamp recording in acute brain slices. (bottom) sample image of eGtACR1-mScarlet expression in NIf.* ***B****) Sample trace (top), raster plot and normalized peri-stimulus time histogram (bottom) reporting the change in multi-unit HVC firing activity in response to light stimulation of eGtACR1-expressing NIf axons in HVC (1s, blue bar).* ***C****) (top) pie charts of the likelihood of observing oEPSCs in HVC_X (cyan), HVC_{RA} (magenta) or HVC_{Av} (yellow). Numbers in the pie fragments are the number of cells in which current (filled) or no current (white) was found. Numbers next to the pie charts are the number of animals. (bottom) stacked bar plot showing the number of cells where both oEPSCs and oIPSCs could be elicited (black), only oEPSCs but no oIPSCs (grey lines), only oIPSCs but no oEPSCs (grey checkers), or neither (white), for each HVC-PN class.* ***D****) box plot and sample traces of oEPSC amplitude per cell class.* ***E****) box plot and sample traces of oIPSC amplitude, by cell class.* ***F****) box plot of the ratio of the second and first oEPSC peak amplitude, by cell class.* ***G****) box plot of the ratio of oEPSC and oIPSC peak amplitude, per cell class.* ***H****) plot (left) and sample traces (right) reporting the amplitude of oEPSCs in ACSF (color), in presence of TTX (black), and after TTX+4AP (gray), by cell class. In traces lacking the TTX trace, TTX and 4AP were washed on at the same time. n= cells, animals. Blue vertical lines show timing of light pulses, 1ms each. Scalebars: 100ms, 100pA.*

Uva monosynaptically innervates HVC_{RA} and HVC_{Av}

Uva is reported to be necessary for song production and its inputs to HVC are thought to be pivotal in this role[21,22]. However, how Uva synaptically influences HVC activity is still poorly understood. We mapped Uva's input to the 3 classes of HVC-PNs. Uva neurons robustly expressed eGtACR1 (**Fig. 3A**). In-vivo extracellular recordings of HVC in anesthetized animals confirmed opsin expression, as indicated by a significant increase in firing activity upon light stimulation (last 100ms baseline vs. last 100ms stim, Wilcoxon matched-pairs signed rank test, $P < 0.0001$, **Fig. 3B**).

In acute brain slices we observed glutamatergic oEPSCs in all retrogradely identified HVC-PN classes, albeit with slightly lower probability than in the NIf inputs described above (60.9% probability (67/110 cells), Fisher's exact test $P = 0.0761$). Optical stimulation of Uva axons resulted in significantly lower probability of observing oEPSCs in HVC_X and HVC_{Av} than in HVC_{RA} neurons (**HVC_X,** 46.9% probability (26/49 cells), average amplitude 142.2±32.0 pA; **HVC_{RA}**, 85.4% probability (35/41 cells), average amplitude 100.5±16.8 pA; **HVC_{Av}**, 45.0% probability (11/19 cells), average amplitude 125.2±52.9 pA. X^2 (2, n = 110) = 16.44, $P = 0.0003$. Kruskal-Wallis test for oEPSC amplitude, H(2) = 1.644, $P = 0.4395$; **Fig. 3C**, **3D**).

In a subset of cells, we also tested the presence of oIPSCs by delivering optical stimulation while holding the membrane voltage to +10mV. We observed GABAergic currents in all three projection subtypes (50% probability (42/84 cells); **HVC_X**, 47.1% probability (16/34 cells), average amplitude 338.7±87.3 pA; **HVC_{RA}**, 79.2% probability (19/24 cells), average amplitude 382.1±115.5 pA; **HVC_{Av}**, 26.9% probability (7/26 cells), average amplitude 202.8±83.9 pA. X^2 (2, n = 84) = 13.82, $P = 0.001$; Kruskal-Wallis test, H(2) = 1.201, $P = 0.5487$, **Fig. 3E**). Like what we observed when stimulating NIf axonal terminals in HVC, Uva axon stimulation yielded oIPSCs mainly in cells where oEPSCs were recorded as well (**HVC_X**, 47.1% oEPSC+oIPSC, 52.9% neither oEPSC nor oIPSC; **HVC_{RA}**, 75% oEPSC+oIPSC, 4.2% oEPSC without oIPSC, 20.8% neither oEPSC nor oIPSC; **HVC_{Av}**, 33.3% oEPSC+oIPSC, 5.6% oIPSC without oEPSC, 61.1% neither oEPSC nor oIPSC; **Fig. 3C**).

The PPR was, similar to what we observed when stimulating NIf terminals, < 1 in the 3 classes of HVC-PNs (**HVC_X**,0.65±0.26; **HVC_{RA}**, 0.37±0.044; **HVC_{Av}**, 0.40±0.16; Kruskal-Wallis, H(2) = 0.9079, $P = 0.6351$; **Fig. 3F**).

The oEPSC/oIPSC ratio was calculated for the cells where both currents were observable (**HVC_X**, 0.73±0.20; **HVC_{RA}**, 0.74±0.19; **HVC_{Av}**, 0.49±0.16; Kruskal-Wallis, H(2) = 0.5490, $P = 0.7599$; **Fig. 3G**).

We then examined which HVC-PN classes receive monosynaptic input from Uva. We found that oEPSC returned after application of TTX+4AP in HVC_{RA} and HVC_{Av} neurons (**HVC_{RA}**, 3/3 cells, 30.7±10.3% of initial response returning after TTX+4AP application; **HVC_{Av}**, 3/3 cells, 55.8±35.8% of initial response returning after TTX+4AP application, **Fig. 3H**). In contrast, we did not observe a monosynaptic current in any of our recordings from HVC_X cells (0/3 cells showing residual current after TTX+4AP application, **Fig. 3H**). We observed oIPSCs being disynaptic or polysynaptic and did not observe monosynaptic oIPSCs in any projection class after application of TTX and 4AP, (**HVC_X**, 0/3 cells tested; **HVC_{RA}**, 0/3 cells tested; **HVC_{Av}**, 0/3 cells tested). Thus, our current mapping shows that Uva provides monosynaptic excitatory input to HVC_{RA} and HVC_{Av} neurons and that it may not project directly to HVC_X neurons.

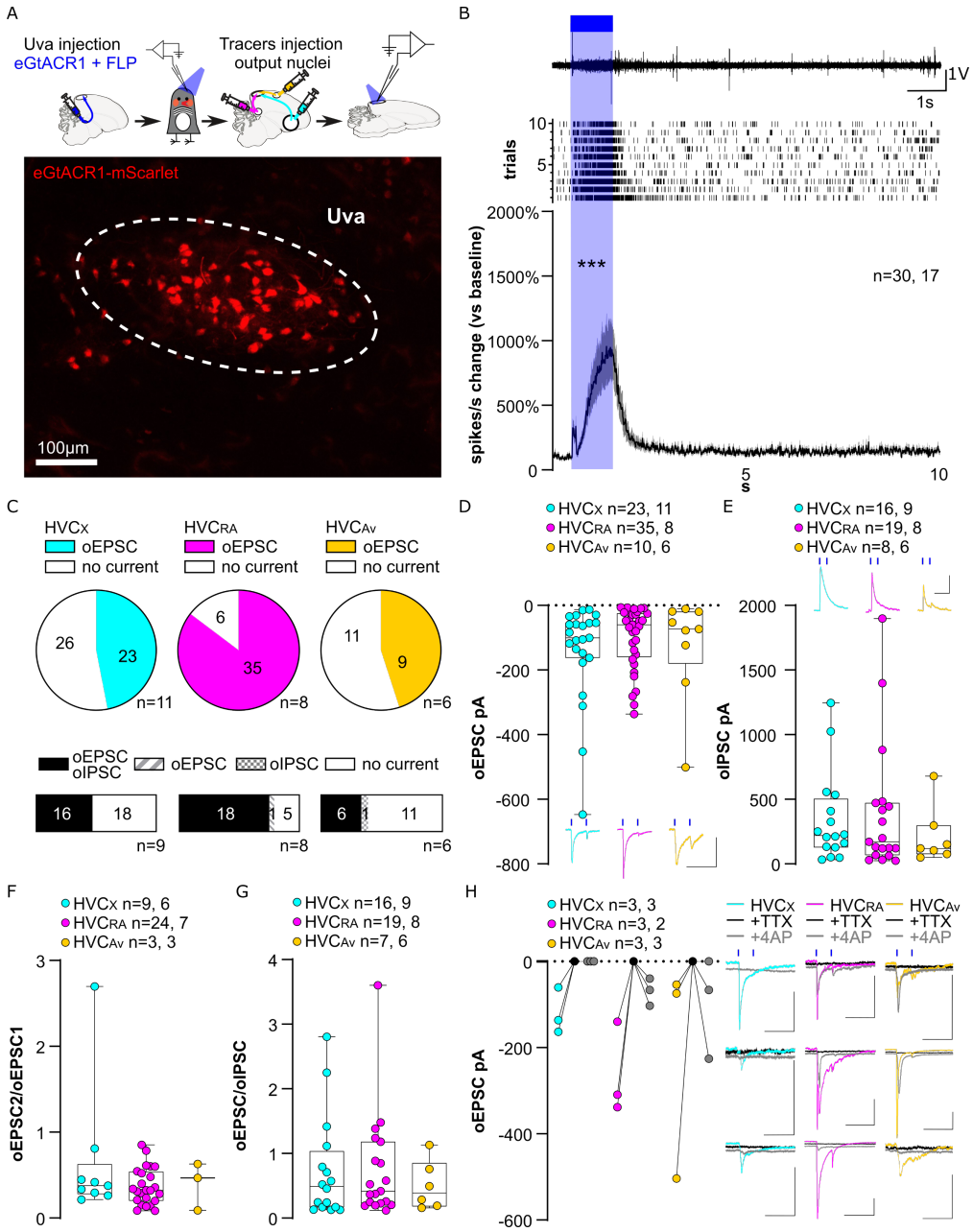

Fig. 3: Uva inputs reliably elicit polysynaptic oIPSCs and oEPSCs in all three HVC-PN classes and monosynaptically connect with HVC_{RA} and HVC_{Av} neurons. A) *(top) Schematic of the experimental timeline, illustrating injection of AAV-CBh-DIO-eGtACR1+ AAV-CBh-FLP in Uva, followed by in-vivo extracellular recording of optically evoked HVC spiking activity in anesthetized birds, retrograde tracer injections in HVC efferent areas and whole-cell patch-clamp recording in acute brain slices. (bottom) sample image of eGtACR1-mScarlet expression in Uva.* ***B)*** *Sample trace (top), raster plot and normalized peri-stimulus time histogram (bottom) reporting the change in multi-unit HVC firing activity in response to light stimulation of eGTACR1-expressing Uva afferents in HVC (1s, blue bar).* ***C)*** *(top) pie charts representing the likelihood of observing oEPSCs in HVC_X (cyan), HVC_{RA} (magenta) or HVC_{Av} (yellow). Numbers in the pie fragments represent the number of cells in which current (filled) or no current (white) was found. Numbers next to the pie charts are the number of animals. (bottom) stacked bar plot showing the number of cells where both oEPSCs and oIPSCs could be elicited (black), only oEPSCs but no oIPSCs (grey lines), only oIPSCs but no oEPSCs (grey checkers), or neither (white), for each HVC-PN class.* ***D)*** *box plot and sample traces of oEPSC amplitude per cell class.* ***E)*** *box plot and sample traces of oIPSC amplitude by cell class.* ***F)*** *box plot of the ratio of the second and first oEPSC peak amplitude by cell class.* ***G)*** *box plot of the ratio of oEPSC and oIPSC peak amplitude, per cell class.* ***H)*** *plot (left) and sample traces (right) reporting the amplitude of oEPSCs in ACSF (color), in presence of TTX (black), and after TTX+4AP (gray), by cell class. In traces lacking the TTX trace, TTX and 4AP were washed on at the same time. n= cells, animals. Blue vertical lines show timing of light pulses, 1ms each. Scalebars: 100ms, 100pA.*

mMAN monosynaptically excites HVC_X and HVC_{Av} neurons

EGtACR1 showed robust expression in mMAN (**Fig. 4A**). In anesthetized birds, light application over HVC resulted in a significant increase in extracellular HVC activity (last 100ms baseline vs. last 100ms stim, Wilcoxon matched-pairs signed rank test, P = 0.0071, **Fig. 4B**).

Upon optical stimulation in brain slices, we found glutamatergic oEPSCs in all retrogradely identified projection neuron classes, albeit with significantly lower success rate compared to what we observed when stimulating NIf terminals (48.6% probability (52/107 cells), Fisher's exact test *P* = 0.0006). oEPSCs were more likely in HVC_X and HVC_{Av} than in HVC_{RA} neurons (**HVC_X**, 59.7% probability (34/57 cells), average amplitude 94.0±11.4 pA; **HVC_{RA}**,27.0% probability (10/37 cells), average amplitude 89.6±31.8 pA; **HVC_{Av}**, 61.5% probability (8/13 cells), average amplitude 144.4±64.4 pA. X^2 (2, n = 107) = 10.55, *P* = 0.0051. Kruskal-Wallis test for oEPSC amplitude, H(2) = 1.537, *P* = 0.4638; **Fig. 4C**, **4D**).

When testing for presence of oIPSCs, we found that optogenetic stimulation of mMAN axonal projections resulted in GABAergic currents in all three HVC-PN classes (53.1% probability (34/64 cells); **HVC_X**, 66.7% probability (20/30 cells); **HVC_{RA}**, 33.3% probability (8/24 cells); **HVC_{Av}**, 53.1% probability (6/10 cells); X^2 (2, n = 64) = 6.174, *P* = 0.0456). We found that oIPSCs in HVC_{Av} had significantly higher amplitude compared to HVC_{RA} (**HVC_X**, 423.4±99.8 pA; **HVC_{RA}**, 317.8±173.8 pA; **HVC_{Av}**, 989.8±310.4 pA; Kruskal-Wallis test, H(2) = 6.800, *P* = 0.0334, Dunn's post-hoc **HVC_{RA} vs. HVC_{Av}** *p* = 0.0288; **Fig. 4E**). oIPSCs were predominantly observed in cells where oEPSCs were also observed, like what we report for NIf and Uva inputs (**HVC_X**, 66.7% oEPSC+oIPSC, 3.3% oEPSC without oIPSC, 30% neither oEPSC nor oIPSC; **HVC_{RA}**, 29.1% oEPSC+oIPSC, 4.2% oIPSC without oEPSC, 66.7% neither oEPSC nor oIPSC; **HVC_{Av}**, 60% oEPSC+oIPSC, 10% oEPSC without oIPSC, 30% neither oEPSC nor oIPSC; **Fig. 4C**).

Similar to what we observed for NIf and Uva inputs, our PPR measures indicated high-probability synaptic release from mMAN afferents to all 3 HVC-PN classes (**HVC_X**, 0.65±0.11; **HVC_{RA}**, 0.45±0.039; **HVC_{Av}**, 0.57±0.088; Kruskal-Wallis, H(2) = 1.564, *P* = 0.4575; **Fig. 4F**).

The E/I ratio highlighted that optogenetic stimulation of mMAN axonal fibers reaching HVC produces relatively stronger GABAergic currents than glutamatergic responses in HVC projection neurons, like what we observed for NIf and Uva input pathways (**HVC_X**, 0.39±0.081; **HVC_{RA}**, 0.77±0.33; **HVC_{Av}**, 0.18±0.033; Kruskal-Wallis, H(2) = 3.181, *P* = 0.2038; **Fig. 4G**).

Finally, we asked whether mMAN monosynaptically contacted any class of HVC-PNs. We found monosynaptic inputs from mMAN onto HVC_X and HVC_{Av} neurons (**HVC_X,** 4/4 cells, 49.0±13.85% of initial response returning after TTX+4AP application; **HVC_{Av}**, 4/4 cells, 34.6±1.5% of initial response returning after TTX+4AP application, **Fig. 4H**). Of the 3 HVC_{RA} neurons tested, 1 exhibited a small monosynaptic current (**HVC_{RA}**, 1/3 cells, 4.4±4.4% average proportion of initial current returning after bath application of TTX+4AP, **Fig. 4H**). We never observed monosynaptic oIPSCs in any projection class after application of TTX and 4AP, indicating that mMAN provides excitatory monosynaptic inputs to HVC (**HVC_X,** 0/4 cells tested, **HVC_{RA},** 0/3 cells tested, **HVC_{Av},** 0/4 cells tested). Together, our current mapping shows that mMAN provides monosynaptic excitatory input to HVC_X and HVC_{Av} neurons. Additional data will be needed to better understand the connectivity between mMAN and HVC_{RA} neurons.

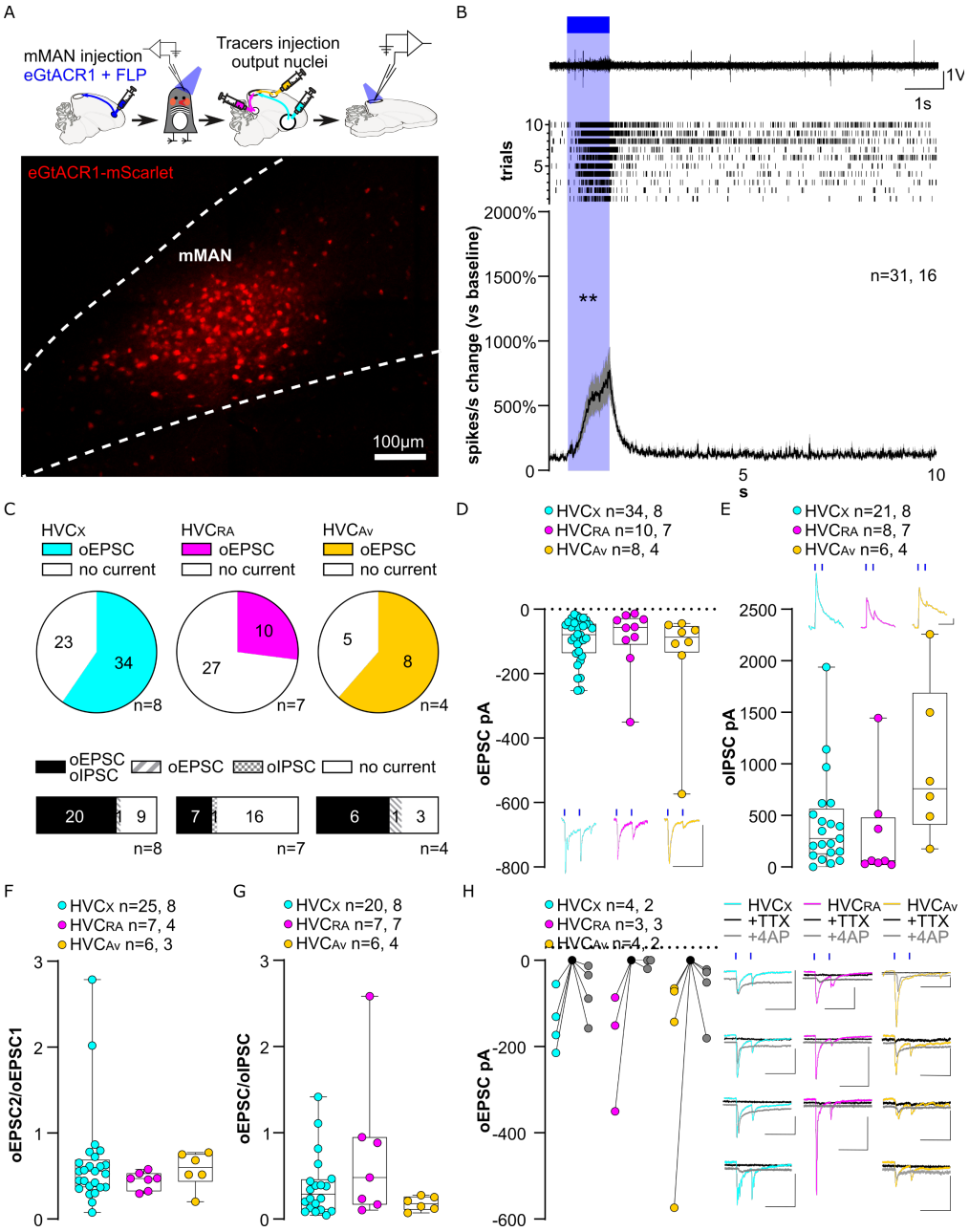

Fig. 4: mMAN inputs elicit polysynaptic oIPSCs and oEPSCs in all three HVC-PN classes and monosynaptically excite HVC_X and HVC_{Av} neurons. A*) (top) Schematic of the experimental timeline, illustrating injection of AAV-CBh-DIO-eGtACR1+ AAV-CBh-FLP in mMAN, followed by in-vivo extracellular recording of optically evoked HVC spiking activity in anesthetized birds, retrograde tracer injections in HVC efferent areas and whole-cell patch-clamp recording in acute brain slices. (bottom) sample image of eGtACR1-mScarlet expression in mMAN.* ***B****) Sample trace (top), raster plot and normalized peri-stimulus time histogram (bottom) reporting the change in multi-unit HVC firing activity in response to light stimulation of eGtACR1-expressing mMAN afferents in HVC (1s, blue bar).* ***C****) (top) pie charts showing the likelihood of observing oEPSCs in HVC_X (cyan), HVC_{RA} (magenta) or HVC_{Av} (yellow). Numbers in the pie fragments represent the number of cells in which current (colored) or no current (white) was found. Numbers next to the pie charts are the number of animals. (bottom) stacked bar plot of the number of cells where both oEPSCs and oIPSCs could be elicited (black), only oEPSCs but no oIPSCs (grey lines), only oIPSCs but no oEPSCs (grey checkers), or neither (white), for each HVC-PN class.* ***D****) box plot and sample traces of oEPSC amplitude per cell class. E) box plot and sample traces of oIPSC amplitude by cell class.* ***F****) box plot of the ratio of the second and first oEPSC peak amplitude by cell class.* ***G****) box plot of the ratio of oEPSC and oIPSC peak amplitude per cell class.* ***H****) plot (left) and sample traces (right) reporting the amplitude of oEPSCs in ACSF (color), in presence of TTX (black), and after TTX+4AP (gray), by cell class . In traces lacking the TTX trace, TTX and 4AP were washed on at the same time. n= cells, animals. Blue vertical lines show timing of light pulses, 1ms each. Scalebars: 100ms, 100pA.*

Av monosynaptically excites HVC_X and HVC_{RA} neurons

Lastly, we mapped the synaptic inputs from Av onto HVC-PNs. Our viral strategy allowed the expression of eGTACR1 in Av neurons, albeit to visibly lower levels than the other inputs examined (**Fig. 5A**). Nonetheless, we confirmed functional expression by optical stimulation of Av axon terminals during in-vivo extracellular recordings from HVC in anesthetized animals (last 100ms baseline vs. last 100ms stim, Wilcoxon matched-pairs signed rank test, P = 0.0008, **Fig. 5B**).

Whole-cell patch-clamp recordings from identified HVC-PN classes in brain slices revealed glutamatergic oEPSCs in all 3 cell classes (38.1% probability (56/147 cells), Fisher's exact test $P < 0.0001$). The likelihood of finding oEPSCs upon Av axon stimulation was similar across the 3 classes of HVC-PNs (**HVC_X**, 39.7% probability (25/63 cells), average amplitude 148.2±36.2 pA; **HVC_{RA}**, 35.6% probability (26/73 cells), average amplitude 125.2±31.1 pA; **HVC_{Av}**, 45.5% probability (5/11 cells), average amplitude 64.02±23.03 pA. X^2 (2, n = 147) = 0.5101, $P = 0.7749$. Kruskal-Wallis test for oEPSC amplitude, H(2) = 1.130, $P = 0.5684$; **Fig. 5C**, **5D**).

When we tested the presence of oIPSCs in a subset of cells and found GABAergic currents in all three projection subtypes (44.9% probability (40/89 cells); **HVC_X**, 48.5% probability (16/33 cells); **HVC_{RA}**, 45.8% probability (22/48 cells); **HVC_{Av}**, 25% probability (2/8 cells); X^2 (2, n = 89) = 1.469, $P = 0.4799$). The average oIPSCs amplitude in HVC_{RA} was significantly lower than found in HVC_X (**HVC_X**, 491.8±117.1 pA; **HVC_{RA}**, 207.9±54.7 pA; **HVC_{Av}**, 56.8±37.8 pA; Kruskal-Wallis test, H(2) = 11.08, $P = 0.0039$, **HVC_X vs. HVC_{RA}** Dunn's post-hoc, p = 0.0088, **Fig. 5E**). As in other pathways already described, we observed oIPSCs mainly in HVC-PNs also showing oEPSCs (**HVC_X**, 48.5% oEPSC+oIPSC, 51.5% neither oEPSC nor oIPSC; **HVC_{RA}**, 39.6% oEPSC+oIPSC, 6.2% oIPSC without oEPSC, 54.2% neither oEPSC nor oIPSC; **HVC_{Av}**, 25% oEPSC+oIPSC, 75% neither oEPSC nor oIPSC; **Fig. 5C**).

Our oEPSCs PPR measures indicated high probability of neurotransmitter release from Av terminals onto the 3 HVC-PN classes (**HVC_X**, 0.41±0.042; **HVC_{RA}**, 0.40±0.076; **HVC_{Av},** 0.30±0.075; Kruskal-Wallis, H(2) = 1.228, $P = 0.5412$; **Fig. 5F**).

The oEPSC/oIPSC ratio, calculated from cells where both currents were observable, showed a significantly higher E/I in HVC_{RA} compared to HVC_X (**HVC_X**, 0.24±0.051; **HVC_{RA}**, 0.69±0.11; **HVC_{Av}**, 2.1±2. 0; Kruskal-Wallis, H(2) = 10.15, $P = 0.0062$, **HVC_X vs. HVC_{RA}** Dunn's post-hoc, p = 0.0052; **Fig. 5G**).

Finally, we examined which HVC-PN neuron classes received monosynaptic input from Av. We consistently observed monosynaptic transmission onto HVC_X and HVC_{RA} but have thus far not observed monosynaptic connections between Av and HVC_{Av} neurons (**HVC_X**, 4/4 cells, 69.0±49.0% of initial response returning after TTX+4AP application; **HVC_{RA}**, 3/4 cells, 19.3±7.1% of initial response returning after TTX+4AP application; **HVC_{Av}**, 0/3 cells showing residual current after TTX+4AP application, **Fig. 5H**). We confirmed the excitatory nature of Av neurotransmission to HVC by observing the lack of oIPSCs after TTX+4AP application, consistent with previous indications[19] (**HVC_X**, 0/4 cells tested; **HVC_{RA}**, 0/2 cells tested; **HVC_{Av}**, 0/1 cells tested). Thus, our current mapping shows that Av provides monosynaptic excitatory input to HVC_{RA} and HVC_X neurons and that it may not project directly onto HVC_{Av} neurons.

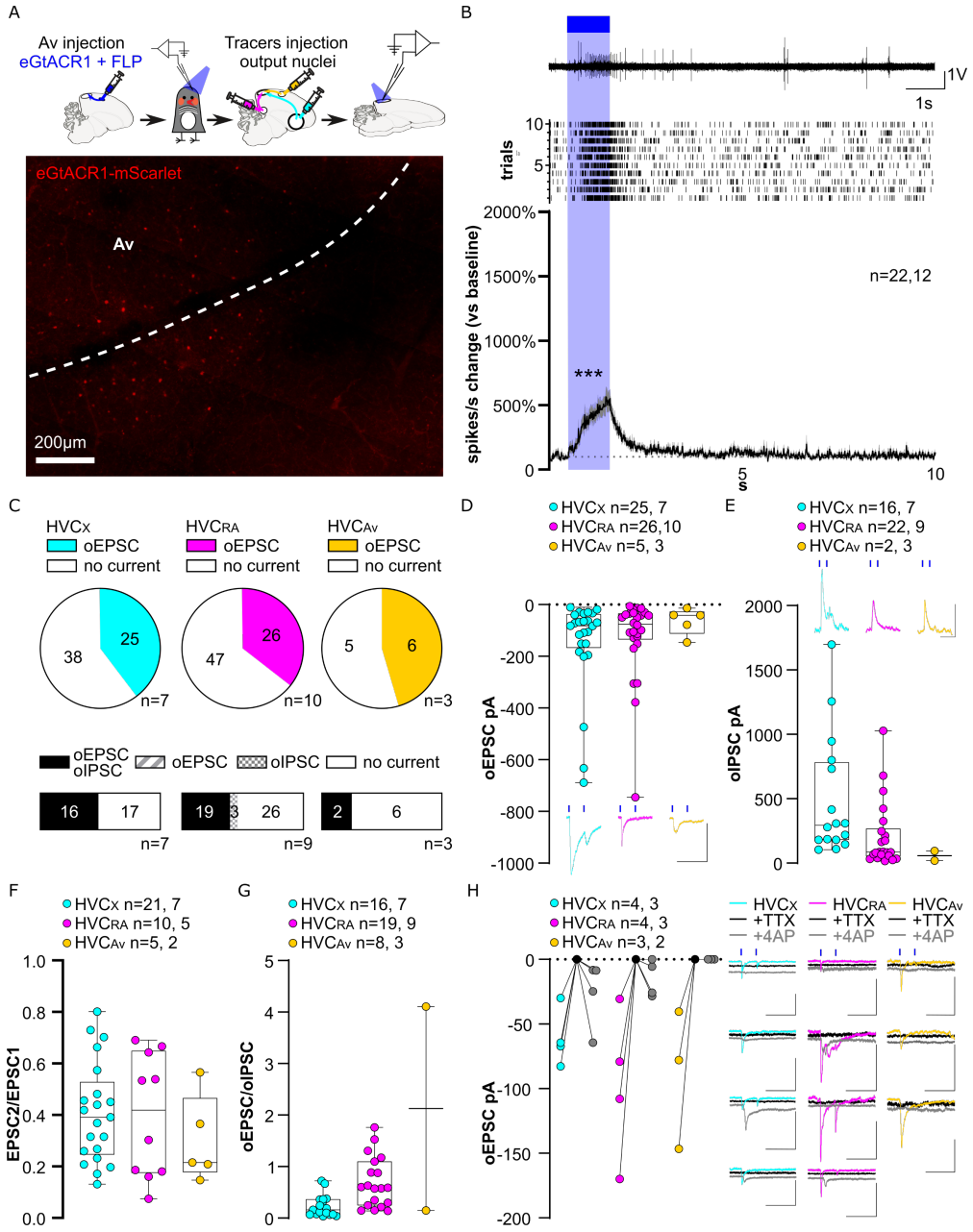

Fig. 5: Av inputs elicit polysynaptic oIPSCs and oEPSCs in all three HVC-PN classes and monosynaptically excite HVC_X and HVC_{RA} neurons. A) *(top) Schematic of the experimental timeline illustrating injection of AAV-CBh-DIO-eGtACR1+ AAV-CBh-FLP in Av, followed by in-vivo extracellular recording of optically evoked HVC spiking activity in anesthetized birds, retrograde tracer injections in HVC efferent areas and whole-cell patch-clamp recording in acute brain slices. (bottom) sample image of eGtACR1-mScarlet expression in Av.* ***B)*** *Sample trace (top), raster plot and normalized peri-stimulus time histogram (bottom) reporting the change in multi-unit HVC firing activity in response to light stimulation of eGtACR1-expressing Av afferents in HVC (1s, blue bar).* ***C)*** *(top) pie charts representing the likelihood of observing oEPSCs in HVC_X (cyan), HVC_{RA} (magenta) or HVC_{Av} (yellow). Numbers in the pie fragments represent the number of cells in which current (filled) or no current (white) was found. Numbers next to the pie charts are the number of animals. (bottom) stacked bar plot of the number of cells where both oEPSCs and oIPSCs could be elicited (black), only oEPSCs but no oIPSCs (grey lines), only oIPSCs but no oEPSCs (grey checkers), or neither (white), for each HVC-PN class.* ***D)*** *box plot and sample traces of oEPSC amplitude per cell class.* ***E)*** *box plot and sample traces of oIPSC amplitude by cell class.* ***F)*** *box plot of the ratio of the second and first oEPSC peak amplitude by cell class.* ***G)*** *box plot of the ratio of oEPSC and oIPSC peak amplitude per cell class.* ***H)*** *plot (left) and sample traces (right) reporting the amplitude of oEPSCs in ACSF (color), in presence of TTX (black), and after TTX+4AP (gray), by cell class n= cells, animals. Blue vertical lines show timing of light pulses, 1ms each. Scalebars: 100ms, 100pA.*

Comparison of Synaptic Inputs to HVC-PNs

By reorganizing the data shown in Fig. **2-5** we examined the probability and strength of oPSCs, within each HVC-PNs class. We find that projection neurons in NIf, Uva, mMAN and Av consistently establish polysynaptic contact with all three HVC-PN classes. We observed both glutamatergic and GABAergic polysynaptic neurotransmission upon afferent axonal terminal stimulation. Organizing our data by HVC-PN classes (**Fig. 6A-F**) we find that HVC_X and HVC_{Av} neurons receive high amplitude oEPSCs from NIf and that HVC_{RA} neurons receive relatively uniform amplitude oEPSCs from all 4 input pathways examined (**HVC_X,** Kruskal-Wallis test, H(3) = 17.93, *P* = 0.0005, **NIf vs Uva** Dunn's post-hoc, p = 0.0117; **NIf vs mMAN** Dunn's post-hoc, p = 0.0001; **NIf vs. Av** Dunn's post-hoc, p = 0.0061; **Fig. 6A**. **HVC_{RA}**, Kruskal-Wallis test, H(3) = 5.821, *P* = 0.1206; **Fig. 6C**. **HVC_{Av}**, Kruskal-Wallis test, H(3) = 7.886, *P* = 0.0484, **NIf vs. Av** Dunn's post-hoc, p = 0.0410; **Fig. 6E**). Stimulation of NIf terminals also resulted in higher amplitude inhibition onto HVC_{Av} neurons than those from Uva or Av (Kruskal-Wallis test, H(3) = 13.17, *P* = 0.0043, **NIf vs. Uva** Dunn's post-hoc, p = 0.0327, **NIf vs. Av** p = 0.0368, **Fig. 6F**). However, we are cautious interpreting results of Av inputs onto HVC_{Av} neurons because this pathway is still under sampled. It is difficult to adequately express eGtACR1 in Av and HVC_{Av} neurons comprise only a small percentage of HVC-PNs, limiting our ability to record from many of these neurons in any single preparation. Finally, while we didn't find any significant difference in the amplitude of optically-evoked post-synaptic currents in HVC_{RA} neurons when stimulating any of the input pathways, we found that Uva stimulation resulted in a significantly higher chance of recording both oEPSCs and oIPSCs in these neurons when compared to the other afferents (oEPSCs, X2 (3, n=175) = 38.53, *P* < 0.0001, **Fig. 6C**; oIPSCs, X2 (3, n=111) = 12.43, *P* = 0.0060, **Fig. 6D**).

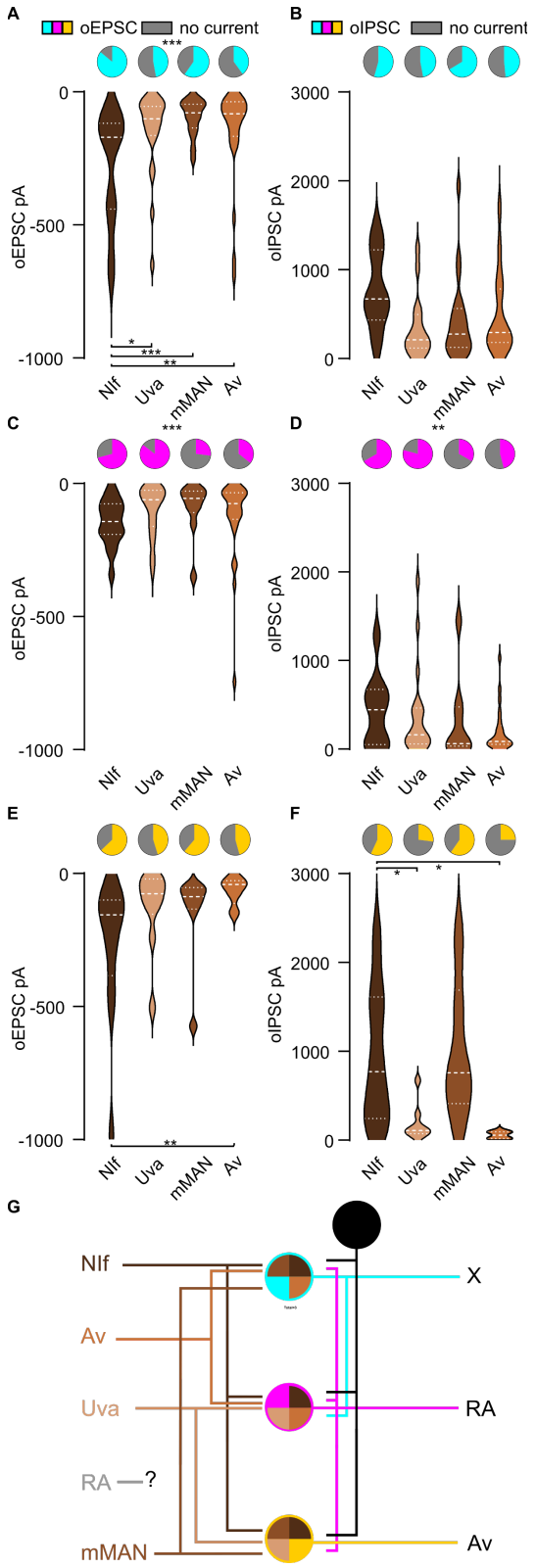

Fig. 6: Summary data organized by PNs and monosynaptic connectivity map HVC afferents. A-F) *Violin plots reporting the data from figure 2-5 reorganized by HVC-PN class, and pie charts representing the likelihood of recording optically evoked currents upon stimulation of the indicated afferent.* ***A)*** *oEPSCs in HVC_X,* ***B)*** *oIPSCs in HVC_X,* ***C)*** *oEPSCs in HVC_{RA},* ***D)*** *oIPSCs in HVC_{RA},* ***E)*** *oEPSCs in HVC_{Av},* ***F)*** *oIPSCs in HVC_{Av}.* ***G)*** *Schematic diagram of the HVC monosynaptic connectivity map revealed in this research (HVC_X cyan, HVC_{RA} magenta, HVC_{Av} yellow, HVC interneurons black).*

Discussion

The songbird motor nucleus HVC is crucial for song production. Its partial or complete lesion results in song disruption and permanent loss, respectively[35-37]. Electrical stimulation of HVC can halt song[38-40]. Further, genetic lesion or manipulation of HVC cell-types and optogenetic or pharmacological manipulations of HVC show that HVC is essential in juvenile song learning [19,41-44]. Despite its importance,

the synaptic organization of HVC's input and output pathways have remained largely unknown. Here, we report the first systematic exploration of functional connectivity between 4 of the 5 input pathways and HVC-PN classes.

Despite our finding that optogenetically driving neurotransmitter release from the 4 input nuclei results in both oEPSCs and oIPSCs, we report that monosynaptic currents, when found, were exclusively excitatory in nature. This confirms that NIf, Uva, mMAN and Av projection neurons to HVC are glutamatergic. While HVC inputs are glutamatergic, our data points towards the existence of a rich interneuronal net that is recruited by these afferent nuclei, therefore providing GABAergic inputs to all HVC-PN classes. This is in line with previous reports that found HVC-PNs activity to be tightly regulated by interneurons[45,46]. However, we report that, across all inputs, the likelihood of finding oIPSCs was tightly dependent on finding oEPSCs in the same cell, possibly suggesting the existence of compartmentalized neuronal ensembles including both PNs and interneurons projecting to those PNs. This model would allow the integration of afferent inputs within a "module" in HVC, providing robustness to the circuit against minimal disruptions such as micro-lesions[47]. A potential caveat is that we performed all our recordings in 230µm thick sagittal brain slices. Day and colleagues have reported that HVC-PNs exhibit sequential activity that is directionally organized in the rostrocaudal axis, while interneurons appear to be coordinated in the medio-lateral axis[48]. Our resection of this mediolateral organization may explain why our optogenetic stimulation elicits oIPSCs mostly in the same neurons where oEPSCs are observed, but not in the others, which may have received inhibition from interneurons sitting in adjacent brain slices.

In addition to finding widespread polysynaptic transmission upon stimulation of any of the afferents, we endeavored to draw a wiring diagram of HVC inputs by isolating the monosynaptic components of these currents. We found surprisingly specific and compartmentalized monosynaptic neurotransmission between each input and HVC-PN classes. NIf terminals monosynaptically contacted all three HVC-PN classes. Uva, instead, appears to monosynaptically contact HVC_{RA} and HVC_{Av}, but may not project directly to HVC_X neurons. We find that mMAN monosynaptically contacts HVC_X and HVC_{Av} neurons but appears to only sparsely project to HVC_{RA} neurons. Finally, Av contacts HVC_X and HVC_{RA}, but may not project directly to HVC_{Av} neurons. At present, our data draws a scenario of multiple intermingled loops coexisting across HVC input and output circuits:

- Thalamic inputs from Uva may directly affect the song motor pathway through monosynaptic projections onto HVC_{RA} neurons. The additional direct inputs to HVC_{Av} neurons are interesting given the proposed role of HVC_{Av} neurons providing a forward model of song to the auditory system[19].
- mMAN preferential connection to HVC_X may create a loop encompassing the thalamus and the AFP. mMAN may integrate RA corollary discharge signals transmitted through DMP. Our findings place mMAN in an ideal position to relay those signals to the AFP, potentially contributing to song plasticity. In addition to its projections to HVC, a separate class of PN in mMAN projects directly to Av (unpublished observations). By contacting HVC_{Av} with one projection neuron subpopulation, and Av with another separate one, mMAN may relay these integrated signals to the auditory system producing a complex monosynaptic-disynaptic integration that will be the subject of future investigations.
- Av neurons do not appear to make monosynaptic connections with HVC_{Av} neurons, potentially ruling out a direct feedback loop between Av and HVC. Nonetheless, NIf provides direct connections with HVC_{Av} neurons and NIf and Av are reciprocally connected, indicating tight sensorimotor loops between cells in these regions and with the AFP.

Ongoing and future directions

While we have traced an initial map of the synaptic connections between the 4 best described afferents to HVC and its 3 projection neuron classes, we are still far from delineating a complete description of HVC afferent and internal circuitry. We are currently in the process of mapping RA projections to the 3 HVC-PN classes and hope to report on this circuitry in the coming months. Another crucial piece of the puzzle is the connectivity of inputs onto the different subclasses of HVC interneurons. Indeed, in the present work we have indirectly described engagement of interneuron populations by stimulating afferent axonal terminals and measuring oIPSCs in HVC-PN classes. While this data allowed us to speculate about possible recruitment of interneurons by each input, a much more detailed and in-depth direct mapping of neurotransmission from these afferents onto HVC interneurons is required. This task is currently made difficult by the absence of reliable transgenic tools allowing us to specifically highlight interneurons with a fluorescent marker for direct ex-vivo recording. While it has been reported that the promoter *mDlx* can be employed to drive the expression of a fluorescent protein in interneurons[49], we have found that constructs driven by the mDlx promoter lack specificity, and

readily express in glutamatergic HVC_X neurons, as well as in some interneurons. Thus, more selective tools are still needed to dissect this circuitry. We have found that eGtACR1 is well suited for mapping long range poly and monosynaptic pathways in zebra finches. Although eGtACR1 is not ideal for mapping local circuit connectivity because it strongly hyperpolarizes somatic and dendritic compartments, expression of other opsins using intersectional viral approaches could prove valuable for high throughput mapping of synaptic connections within HVC.

While our opsin-assisted circuit mapping provides us with a new level of insight into HVC synaptic circuitry, there are caveats and limitations to this approach that should be considered:

- Ex-vivo brain slices have historically been demonstrated to be a reliable window into neuronal and circuit function. However intrinsic activity patterns of some neuronal subtypes are known to change in acute slices[50]. Moreover, the slicing procedure severs both neuromodulatory and neurotransmitter afferents, potentially attenuating or removing synaptic inputs to some circuits[51].
- Our axonal terminal optical manipulation recruits all the fibers expressing eGtACR1 under the cone of light of the microscope objective. Therefore, our estimates of postsynaptic responses and likelihood of finding responses are based on the simultaneous release of neurotransmitter from all the afferent terminals expressing eGtACR1, and they should be understood in this context. Future studies will need to employ conditions of minimal stimulation that may further characterize the specific properties of monosynaptic and polysynaptic neurotransmission in the examined inputs.
- The use of eGtACR1, while granting high amplitude photocurrents, limits our ability to precisely study synaptic properties due to its slow off kinetics (≈ 100ms)[32,33,52]. This directly affects the steady state of the presynaptic terminals, especially upon multiple stimulations in a short timeframe (such as our protocol for PPR calculation). Future studies may circumvent this limitation by employing faster kinetic opsins (e.g. ChETA, Chronos, ChroME)[25,53,54].
- Our opsin assisted circuit mapping depended on the ability transduce neurons with AAV in 4 different brain pathways. There can be variability in viral expression between animals and among different brain pathways, and our understanding of viral tropism across the song circuit is still limited. Considering these caveats, we expect there to be updates and refinement to this first wiring diagram.
- Here we report on our recordings from 435 HVC-PNs and 4 input pathways. Of these we believe that we need more recordings of the Av to HVC circuit. Interrogation of Av projections has proved challenging, particularly recordings of Av projections onto HVC_{Av} neurons.
- While the synaptic transmission between an afferent and each class of HVC-PN tended to be homogeneously either mono- and polysynaptic, or only polysynaptic, it is possible that with more recordings we or others will reveal additional monosynaptic connections in this circuit.

Our first step in the direction of a complete synaptic functional mapping of HVC afferent and efferent circuits provides us with a complex picture of clustered and interconnected neuronal ensembles, each composed of HVC-PN classes integrating segregated information from thalamic, auditory, and motor areas. Our hope is that this resource, and its continued development, will be useful to the many researchers working to understand how this core circuit functions as birds learn to imitate and precisely control their song.

Materials and Methods

Animals

Experiments described in this study were conducted using adult male zebra finches (130-500 days post hatch (dph)). All procedures were performed in accordance with protocols approved by Animal Care and Use Committee at UT Southwestern Medical Center.

Viral Vectors

The following adeno-associated viral vectors were used in these experiments: rAAV2/9/CBh-FLP and rAAV-CBh-eGTACR1-mScarlet (IDDRC Neuroconnectivity Core at Baylor College of Medicine). All viral vectors were aliquoted and stored at -80°C until use.

Constructs

CBh-eGTACR1-mScarlet was generated by inserting KpnI and AgeI restriction sites flanking EF1a in the pAAV-EF1a-F-FLEX-mNaChBac-T2A-tdTomato (a gift from Dr. Massimo Scanziani; Addgene plasmid # 60658) through pcr cloning. The CBh promoter was isolated from pX330-U6-Chimeric_BB-CBh-hSpCas9 (a gift from Dr. Feng Zhang; Addgene plasmid # 42230) by digestion of the KpnI and AgeI restriction sites and inserted into the KpnI/AgeI restriction sites of the pAAV-EF1a-F-FLEX-mNaChBac-T2A-tdTomato backbone. Next, we isolated mScarlet from pmScarlet_C1 (a gift from Dr. Dorus Gadella; Addgene plasmid # 85042) through pcr amplification, inserting a BamHI restriction site into the 5' end of the ORF. We digested the amplified fragments with BamHI and BsrGI, inserting the digested fragments into BamHI/BsrGI restriction sites of the pAAV-CBh-F-FLEX-mNaChBac-T2A-tdTomato backbone. eGTACR1 was then amplified from pAAV-CAG-DIO-NLS-mRuby3-IRES-eGTACR1-ST (a gift from Dr. Hillel Adesnik; Addgene plasmid # 109048) with a BmtI restriction site on the 5' end and a AflII restriction site on the 3'end, avoiding amplification of the soma-targeting sequence in the original plasmid. We then digested the amplified fragment with BmtI and AflII, inserting the fragment into the BmtI/AflII sites of the pAAV-CBh-F-FLEX-mNaChBac-T2A-mScarlet.

For CBh- Flpo, we amplified the FLP ORF from pCAG- Flpo (a gift from Dr. Massimo Scanziani; Addgene plasmid # 60662) with a AgeI restriction site on the 5' end. We then digested the amplified fragment with AgeI and EcoRI, inserting the fragment into the AgeI/EcoRI sites of the CBh-eGTACR1-mScarlet.

Constructs were verified with Sanger sequencing.

Stereotaxic Surgery

All surgical procedures were performed under aseptic conditions. Birds were anaesthetized using isoflurane inhalation (0.8-1.5%) and placed in a stereotaxic surgical apparatus.

Viral injections were performed using previously described procedures[19,41]. Briefly, a cocktail of adeno-associated viral vectors (1:2 of rAAV-CBh-FLP and rAAV-DIO-CBh-eGTACR1, respectively) were injected into NIf, UVA, mMAN and Av (1nl/s, for a total of 1.5 µl/hemisphere). Experiments were conducted starting a minimum of 4 weeks after viral injections. Fluorophore-conjugated retrograde tracers (Dextran 10,000MW, AlexaFluor 488 and 568, Invitrogen; FastBlue, Polisciences) were injected bilaterally into birds' Area X, Av, and RA. Tracer injections (160nl, 5x32 n, 32nl/s every 30 s) were performed using previously described procedures[19,41,55]. The centers of HVC, NIf, mMAN and RA were identified with electrophysiological recordings, and Area X, Av and UVA were identified using stereotaxic coordinates (approximate stereotaxic coordinates relative to interaural zero and the brain surface: head angle, rostral-caudal, medial-lateral, dorsal-ventral (in mm). HVC: 45°, AP 0, ML ±2.4, DV -0.2-0.6; NIf: 45°, AP 1.75, ML ± 1.75, DV -2.4 -1.8; mMAN: 20°, AP 5.1, ML ±0.6, DV -2.1 -1.6; RA: 70°, AP -1.5, ML ± 2.5, DV -2.4 -1.8; X: 45°, AP 4.6, ML ±1.6, DV -3.3 -2.7; Av: 45°, AP 1.65, ML ± 2.0, DV -0.9; UVA: 20°, AP 2.8, ML ±1.6, DV -4.8 -4.2).

***In-vivo* extracellular recordings**

To test the functional expression of eGtACR1 in HVC afferents, and to characterize the effects of optogenetic stimulation of neurotransmitter release from those onto HVC neurons, we performed extracellular recording of HVC activity in anesthetized birds formerly injected with rAAV-DIO-CBh-eGtACR1 and rAAV-CBh-FLP (2:1) in HVC afferent areas. We performed the recordings under light isoflurane anesthesia (0.8%) with Carbostar carbon electrodes (impedance: 1670 microhms/cm; Kation Scientific). During the recordings, we lowered a 400µm multimodal optical fiber to the brain surface overlaying HVC and delivered light stimulation (470nm, ≈20mW, 1s). Signals were acquired at 10KHz, and filtered (high-pass 300Hz, low-pass 20KHz). We used Spike2 to analyze the spike rate (binned every 10ms) and build a peri-stimulus time histogram to evaluate the effect of light stimulation across trials (5-15 trials/hemisphere). We sampled a minimum of 1 site and a maximum of 3 HVC sites/hemisphere. Birds with weak or no optically evoked responses were excluded from experiments. For hemispheres showing light-evoked responses, spike counts from peri-stimulus time histograms were normalized to the pre-stimulus baseline (500ms).

***Ex vivo* physiology**

Slice preparation.

Zebra finches were deeply anesthetized with isoflurane and decapitated. The brain was removed from the skull and submerged in cold (1– 4°C) oxygenated dissection buffer. Acute sagittal 230 µm brain slices were cut in ice-cold carbogenated (95% O2/5% CO2) solution, containing (in mM) 110 choline chloride, 25 glucose, 25 NaHCO3, 7 MgCl2, 11.6 ascorbic acid, 3.1 sodium pyruvate, 2.5 KCl, 1.25 NaH2PO4, 0.5 CaCl2; 320-330 mOsm. Individual slices were incubated in a custom-made holding chamber filled with artificial cerebrospinal fluid (aCSF), containing (in mM): 126 NaCl, 3 KCl, 1.25

NaH_2PO_4, 26 $NaHCO_3$, 10 D-(+)-glucose, 2 $MgSO_4$, 2 $CaCl_2$, 310mOsm, pH 7.3–7.4, aerated with a 95% O_2/5% CO_2 mix. Slices were incubated at 36 °C for 20 minutes, and then kept at RT for a minimum of 45 minutes before recordings.

Slice electrophysiological recording.

Slices were constantly perfused in a submersion chamber with 32°C oxygenated normal aCSF. Patch pipettes were pulled to a final resistance of 3-5 MΩ from filamented borosilicate glass on a Sutter P-1000 horizontal puller. HVC-PN classes, as identified by retrograde tracers, were visualized by epifluorescence imaging using a water immersion objective (×40, 0.8 numerical aperture) on an upright Olympus BX51 WI microscope, with video-assisted infrared CCD camera (Q-Imaging Rolera). Data were low-pass filtered at 10 kHz and acquired at 10 kHz with an Axon MultiClamp 700B amplifier and an Axon Digidata 1550B Data Acquisition system under the control of Clampex 10.6 (Molecular Devices).

For voltage clamp whole-cell recordings, the internal solution contained (in mM): 120 cesium methanesulfonate, 10 CsCl, 10 HEPES, 10 EGTA, 5 Creatine Phosphate, 4 ATP-Mg, 0.4 GTP-Na (adjusted to pH 7.3-7.4 with CsOH).

Optically evoked synaptic currents were measured by delivering 2 light pulses (1 ms, spaced 50ms, generated by a CoolLED *p*E300) focused on the sample through the 40X immersion objective. Sweeps were delivered every 10 s. Synaptic responses were monitored while holding the membrane voltage at -70mV (for oEPSCs) and +10mV (for oIPSCs). We monitored different light stimulation intensities prior to baseline recording to achieve oEPSCs responses at ~50% of the maximal response. Access resistance (10–30 MΩ) was monitored throughout the experiment, and recordings where it changed more than 20% were discarded from further analysis. We calculated the PPR as the amplitude of the second peak divided by the amplitude of the first peak elicited by the twin stimuli. The E/I ratio was calculated by dividing the amplitude of the oEPSC at -70mV by the amplitude of the oIPSC at +10mV, while stimulating at identical light intensities. To validate inhibitory and excitatory PSCs as GABAergic and glutamatergic, respectively, in a subset of cells we bath applied the GABAa receptor antagonist SR 95531 hydrobromide (gabazine, µM) while holding the cell at +10mV, or the AMPA receptor antagonist 6,7-Dinitroquinoxaline-2,3-dione (DNQX, µM) while holding the cell at -70mV. In another subset of cells, once the baseline measures were established, we tested for monosynaptic connectivity. To isolate monosynaptic currents driven by optogenetic stimulation we bath applied 1µM Tetrodotoxin (TTX), followed by 100µM 4-Aminopyridine (4AP) and measured the amplitude of PSCs returning following 4-AP application. Currents under 5pA were considered not reliable, based on the S/N of the recordings, and were assigned value 0 for further analysis. For sake of classification, if any current rescued by 4AP application had amplitude lower than 5% of the baseline value it was considered non-monosynaptic and was given value 0.

Histology

After electrophysiological recordings, the slices were incubated in 4% PFA in PBS. Sections were then washed in PBS, mounted on glass slides with Fluoromount-G (eBioscience, CA, USA), and visualized under an LSM 880 laser-scanning confocal microscope (Carl Zeiss, Germany).

Statistical Analysis

All data were tested for normality using the Shapiro-Wilk Test. Parametric and non-parametric statistical tests were used as appropriate. One-way Anova or Kruskal-Wallis test was performed when comparisons were made across more than two conditions. Fisher or X^2 tests, followed by Dunn's post-hoc test, were used to compare the probability of finding optically evoked responses across the HVC-PN classes while stimulating the different afferents. Statistical significance refers to *$P < 0.05$, ** $P < 0.01$, *** $P < 0.001$.

Acknowledgments

We thank Drs. David Perkel, Frank Meye, Jay Gibson, Salvatore Lecca and Manuel Mameli for discussion and comments on the manuscript. Andrea Guerrero, Luis Garcia, and Jennifer Holdway for laboratory support. This research was supported by grants from the US National Institutes of Health UF1NS115821 and R01NS108424 to TFR. DA is supported by F99NS124172. All authors conceived the project. TFR supervised the research. MT and TFR designed the experiments and wrote the manuscript with input from DA. MT collected and analyzed the data for the project. DA designed and optimized viral tools used in this research and helped develop scripts for analysis of electrophysiological data. All authors read and commented on the manuscript. Authors declare no competing interests. All data is available in the main text or the supplementary materials.

References

1 Immelmann, K. in *Bird Vocalisations* (ed R.A. Hinde) 61-74 (Cambridge University Press, 1969).

2 Price, P. H. Developmental determinants of structure in zebra finch song. *Journal of Comparative and Physiological Psychology* **93**, 260-277 (1979).

3 Sossinka, R. & Bohner, J. Song types in the zebra finch *Poephila guttata castanotis*. *Zeitschrift fur Tierpsychologie* **53**, 123-132 (1980).

4 Bohner, J. Song learning in the zebra finch (Taeniopygia guttata): selectivity in choice of a tutor and accuracy of song copies. *Animal Behavior* **31**, 231-237 (1983).

5 Zann, R. A. Structural variation in the zebra finch distance call. *Zeitschrift fur Tierpsychologie* **66**, 328-345 (1984).

6 Clayton, N. S. Song learning in cross-fostered zebra finches: A re-examination of the sensitive phase. *Behaviour* **102**, 67-81 (1987).

7 Bohner, J. Early acquisition of song in the zebra finch, *Taeniopygia guttata*. *Animal Behavior* **39**, 369-374 (1990).

8 Zann, R. A. *The Zebra Finch: a Synthesis of Field and Laboratory Studies*. (Oxford University Press, 1996).

9 Tchernichovski, O., Lints, T., Mitra, P. P. & Nottebohm, F. Vocal imitation in zebra finches is inversely related to model abundance. *Proc Natl Acad Sci U S A* **96**, 12901-12904 (1999).

10 Tchernichovski, O., Mitra, P. P., Lints, T. & Nottebohm, F. Dynamics of the vocal imitation process: how a zebra finch learns its song. *Science* **291**, 2564-2569 (2001).

11 Funabiki, Y. & Konishi, M. Long memory in song learning by zebra finches. *J Neurosci* **23**, 6928-6935 (2003).

12 Goller, F. & Cooper, B. G. Peripheral motor dynamics of song production in the zebra finch. *Ann N Y Acad Sci* **1016**, 130-152 (2004). https://doi.org:10.1196/annals.1298.009

13 Nottebohm, F., Stokes, T. M. & Leonard, C. M. Central control of song in the canary, *Serinus canarius*. *Journal of Comparative Neurology* **165**, 457-486 (1976).

14 Konishi, M. Birdsong for neurobiologists. *Neuron* **3**, 541-549 (1989).

15 Schmidt, M. F. & Goller, F. Breathtaking Songs: Coordinating the Neural Circuits for Breathing and Singing. *Physiology (Bethesda)* **31**, 442-451 (2016). https://doi.org:10.1152/physiol.00004.2016

16 Schmidt, M. F., Ashmore, R. C. & Vu, E. T. Bilateral control and interhemispheric coordination in the avian song motor system. *Ann N Y Acad Sci* **1016**, 171-186 (2004).

17 Mooney, R. Neural mechanisms for learned birdsong. *Learn Mem* **16**, 655-669 (2009). https://doi.org:10.1101/lm.1065209

18 Fee, M. S., Kozhevnikov, A. A. & Hahnloser, R. H. Neural mechanisms of vocal sequence generation in the songbird. *Ann N Y Acad Sci* **1016**, 153-170 (2004).

19 Roberts, T. F. *et al.* Identification of a motor-to-auditory pathway important for vocal learning. *Nat Neurosci* **20**, 978-986 (2017). https://doi.org:10.1038/nn.4563

20 Foster, E. F. & Bottjer, S. W. Lesions of a telencephalic nucleus in male zebra finches: Influences on vocal behavior in juveniles and adults. *J Neurobiol* **46**, 142-165 (2001). https://doi.org:10.1002/1097-4695(20010205)46:2<142::aid-neu60>3.0.co;2-r

21 Danish, H. H., Aronov, D. & Fee, M. S. Rhythmic syllable-related activity in a songbird motor thalamic nucleus necessary for learned vocalizations. *PLoS One* **12**, e0169568 (2017). https://doi.org:10.1371/journal.pone.0169568

22 Coleman, M. J. & Vu, E. T. Recovery of impaired songs following unilateral but not bilateral lesions of nucleus uvaeformis of adult zebra finches. *J Neurobiol* **63**, 70-89 (2005). https://doi.org:10.1002/neu.20122

23 Hamaguchi, K. & Mooney, R. Recurrent interactions between the input and output of a songbird cortico-basal ganglia pathway are implicated in vocal sequence variability. *J Neurosci* **32**, 11671-11687 (2012). https://doi.org:10.1523/jneurosci.1666-12.2012

24 Hamaguchi, K., Tanaka, M. & Mooney, R. A Distributed Recurrent Network Contributes to Temporally Precise Vocalizations. *Neuron* **91**, 680-693 (2016). https://doi.org:10.1016/j.neuron.2016.06.019

25 Mardinly, A. R. *et al.* Precise multimodal optical control of neural ensemble activity. *Nat Neurosci* **21**, 881-893 (2018). https://doi.org:10.1038/s41593-018-0139-8

26 Govorunova, E. G., Sineshchekov, O. A., Janz, R., Liu, X. & Spudich, J. L. NEUROSCIENCE. Natural light-gated anion channels: A family of microbial rhodopsins for advanced optogenetics. *Science* **349**, 647-650 (2015). https://doi.org:10.1126/science.aaa7484

27 Malyshev, A. Y. *et al.* Chloride conducting light activated channel GtACR2 can produce both cessation of firing and generation of action potentials in cortical neurons in response to light. *Neurosci Lett* **640**, 76-80 (2017). https://doi.org:10.1016/j.neulet.2017.01.026
28 Messier, J. E., Chen, H., Cai, Z. L. & Xue, M. Targeting light-gated chloride channels to neuronal somatodendritic domain reduces their excitatory effect in the axon. *Elife* **7** (2018). https://doi.org:10.7554/eLife.38506
29 Khirug, S. *et al.* GABAergic depolarization of the axon initial segment in cortical principal neurons is caused by the Na-K-2Cl cotransporter NKCC1. *J Neurosci* **28**, 4635-4639 (2008). https://doi.org:10.1523/jneurosci.0908-08.2008
30 Linders, L. E. *et al.* Studying Synaptic Connectivity and Strength with Optogenetics and Patch-Clamp Electrophysiology. *Int J Mol Sci* **23** (2022). https://doi.org:10.3390/ijms231911612
31 Petreanu, L., Mao, T., Sternson, S. M. & Svoboda, K. The subcellular organization of neocortical excitatory connections. *Nature* **457**, 1142-1145 (2009). https://doi.org:10.1038/nature07709
32 Mahn, M. *et al.* High-efficiency optogenetic silencing with soma-targeted anion-conducting channelrhodopsins. *Nat Commun* **9**, 4125 (2018). https://doi.org:10.1038/s41467-018-06511-8
33 Ochs, A. R., Karathanos, T. V., Trayanova, N. A. & Boyle, P. M. Optogenetic Stimulation Using Anion Channelrhodopsin (GtACR1) Facilitates Termination of Reentrant Arrhythmias With Low Light Energy Requirements: A Computational Study. *Front Physiol* **12**, 718622 (2021). https://doi.org:10.3389/fphys.2021.718622
34 Coleman M. J., M. R. Synaptic transformations underlying highly selective auditory representations of learned birdsong. *J. Neurosci.*, Aug 18;24(33):7251-7265. doi: 7210.1523/JNEUROSCI.0947-7204.2004. (2004).
35 Simpson, H. B. & Vicario, D. S. Brain pathways for learned and unlearned vocalizations differ in zebra finches. *J Neurosci* **10**, 1541-1556 (1990). https://doi.org:10.1523/jneurosci.10-05-01541.1990
36 Aronov, D., Andalman, A. S. & Fee, M. S. A specialized forebrain circuit for vocal babbling in the juvenile songbird. *Science* **320**, 630-634 (2008). https://doi.org:10.1126/science.1155140
37 Basista, M. J. *et al.* Independent premotor encoding of the sequence and structure of birdsong in avian cortex. *J Neurosci* **34**, 16821-16834 (2014). https://doi.org:10.1523/jneurosci.1940-14.2014
38 Vu, E. T., Mazurek, M. E. & Kuo, Y. C. Identification of a forebrain motor programming network for the learned song of zebra finches. *J Neurosci* **14**, 6924-6934 (1994). https://doi.org:10.1523/jneurosci.14-11-06924.1994
39 Ashmore, R. C., Wild, J. M. & Schmidt, M. F. Brainstem and forebrain contributions to the generation of learned motor behaviors for song. *J Neurosci* **25**, 8543-8554 (2005). https://doi.org:10.1523/jneurosci.1668-05.2005
40 Vu, E. T., Schmidt, M. F. & Mazurek, M. E. Interhemispheric coordination of premotor neural activity during singing in adult zebra finches. *J Neurosci* **18**, 9088-9098 (1998). https://doi.org:10.1523/jneurosci.18-21-09088.1998
41 Roberts, T. F., Gobes, S. M., Murugan, M., Ölveczky, B. P. & Mooney, R. Motor circuits are required to encode a sensory model for imitative learning. *Nat Neurosci* **15**, 1454-1459 (2012). https://doi.org:10.1038/nn.3206
42 Garcia-Oscos, F. *et al.* Autism-linked gene FoxP1 selectively regulates the cultural transmission of learned vocalizations. *Sci Adv* **7** (2021). https://doi.org:10.1126/sciadv.abd2827
43 Sánchez-Valpuesta, M. *et al.* Corticobasal ganglia projecting neurons are required for juvenile vocal learning but not for adult vocal plasticity in songbirds. *Proc Natl Acad Sci U S A* **116**, 22833-22843 (2019). https://doi.org:10.1073/pnas.1913575116
44 Tanaka, M., Sun, F., Li, Y. & Mooney, R. A mesocortical dopamine circuit enables the cultural transmission of vocal behaviour. *Nature* **563**, 117-120 (2018). https://doi.org:10.1038/s41586-018-0636-7
45 Kosche, G., Vallentin, D. & Long, M. A. Interplay of inhibition and excitation shapes a premotor neural sequence. *J Neurosci* **35**, 1217-1227 (2015). https://doi.org:10.1523/jneurosci.4346-14.2015
46 Vallentin, D., Kosche, G., Lipkind, D. & Long, M. A. Neural circuits. Inhibition protects acquired song segments during vocal learning in zebra finches. *Science* **351**, 267-271 (2016). https://doi.org:10.1126/science.aad3023
47 Stauffer, T. R. *et al.* Axial organization of a brain region that sequences a learned pattern of behavior. *J Neurosci* **32**, 9312-9322 (2012). https://doi.org:10.1523/jneurosci.0978-12.2012
48 Day, N. F., Terleski, K. L., Nykamp, D. Q. & Nick, T. A. Directed functional connectivity matures with motor learning in a cortical pattern generator. *J Neurophysiol* **109**, 913-923 (2013). https://doi.org:10.1152/jn.00937.2012
49 Dimidschstein, J. *et al.* A viral strategy for targeting and manipulating interneurons across vertebrate species. *Nat Neurosci* **19**, 1743-1749 (2016). https://doi.org:10.1038/nn.4430

50 Opitz, A., Falchier, A., Linn, G. S., Milham, M. P. & Schroeder, C. E. Limitations of ex vivo measurements for in vivo neuroscience. *Proc Natl Acad Sci U S A* **114**, 5243-5246 (2017). https://doi.org:10.1073/pnas.1617024114

51 Ballanyi, K. & Ruangkittisakul, A. in *Encyclopedia of Neuroscience* (eds Marc D. Binder, Nobutaka Hirokawa, & Uwe Windhorst) 483-490 (Springer Berlin Heidelberg, 2009).

52 Kim, Y. S. *et al.* Crystal structure of the natural anion-conducting channelrhodopsin GtACR1. *Nature* **561**, 343-348 (2018). https://doi.org:10.1038/s41586-018-0511-6

53 Gunaydin, L. A. *et al.* Ultrafast optogenetic control. *Nat Neurosci* **13**, 387-392 (2010). https://doi.org:10.1038/nn.2495

54 Klapoetke, N. C. *et al.* Independent optical excitation of distinct neural populations. *Nat Methods* **11**, 338-346 (2014). https://doi.org:10.1038/nmeth.2836

55 Xiao, L. *et al.* A Basal Ganglia Circuit Sufficient to Guide Birdsong Learning. *Neuron* **98**, 208-221.e205 (2018). https://doi.org:10.1016/j.neuron.2018.02.020